Scripta Materialia 139 (2017) 1–4

Contents lists available at ScienceDirect

Scripta Materialia

journal homepage: www.elsevier.com/locate/scriptamat

Regular Article

Diffusion of point defects near stacking faults in 3C-SiC via first-principles calculations

Jianqi Xi [a], Bin Liu [b], Fenglin Yuan [c], Yanwen Zhang [d,a], William J. Weber [a,d,*]

[a] Department of Materials Science and Engineering, University of Tennessee, Knoxville, TN 37996, USA
[b] School of Materials Science and Engineering, Shanghai University, Shanghai 200444, China
[c] Department of Materials Science and Engineering, Johns Hopkins University, Baltimore, MD 21218, USA
[d] Materials Science and Technology Division, Oak Ridge National Laboratory, Oak Ridge, TN 37831, USA

ARTICLE INFO

Article history:
Received 8 March 2017
Received in revised form 31 May 2017
Accepted 4 June 2017
Available online 12 June 2017

Keywords:
Stacking faults
Point defects
First-principles calculations
Diffusion
Silicon carbide

ABSTRACT

First-principles calculations are used to investigate diffusion of point defects near stacking faults in 3C-SiC and to identify the migration mechanisms. Compared with the energy barriers for defects in the bulk, the migration barriers for both Si and C vacancies and Si interstitials near the stacking fault are found to decrease. For C interstitials, the energy barriers increase depending on the electronic localization in the stacking fault region. The lower barriers for Si interstitial diffusion near the faults may be responsible for the enhanced defect annihilation observed under irradiation in 3C-SiC with high densities of stacking faults.

Nanostructured ceramics have opened new and fascinating avenues for research in nuclear applications due to excellent radiation-resistant properties. The increased volume fraction of disordered intergranular regions or interfaces in these materials, such as grain boundaries (GBs) and stacking faults (SFs), plays a critical role in damage evolution under irradiation [1–17]. Nanocrystalline (NC) materials with high-densities of grain boundaries are believed to have substantially different response to radiation damage as compared to the response of microcrystalline materials [1–8]. Enhanced self-healing has been reported for NC materials, such as Pd [4], $MgGa_2O_4$ [5], CeO_2 [6], and YSZ [7,8], due to the increased grain boundary densities, which significantly improve the radiation resistance compared with microcrystalline materials. However, results from molecular dynamics simulations [9–11] and experiments [12,13] in NC-SiC are somewhat contradictory, suggesting that the influence of GBs on damage evolution in irradiated NC materials remains unclear. Meanwhile, the influence of SFs in materials on radiation response has also been identified [14–17]. Zhang et al. [14,15] reported improved radiation-resistant behavior in nano-engineered SiC (NE-SiC) with high stacking fault (SF) densities. A recent study by Imada et al. [17] has provided further experimental evidence on the important role of the unique nanolayered structure in improving the radiation tolerance of NE-SiC.

Although it has been suggested that enhanced defect recombination and annihilation rates are associated with the presence of the SFs in NE-SiC, no clear atomic-level picture explains why irradiation-induced defects are more readily annihilated in NE-SiC than in the bulk. On the theoretical side, Jamison et al. [18] studied the formation and migration of native point defects near SFs in 3C-SiC. Their results suggested that SFs have no effect on the defect configurations and that all intrinsic defects were in the neutral charge state; their conclusion was that the migration barriers of defects decreased near the SFs. However, our recent work [19] showed that, after considering the charge redistribution between SFs and defects, the existence of SFs in 3C-SiC strongly changes the configurations of point defects, especially Si interstitials, modifying the energy landscape near the SFs, which may affect the migration behavior of these defects, and consequently influence defect annihilation processes.

In order to better understand the effect of interactions between SFs and defects on the recovery of irradiation-induced defects, the migration behavior of native point defects near the SFs is systematically investigated using first-principles calculations. For comparison, the calculations are also performed on the migration of these defects in bulk 3C-SiC. In the present work, diffusion pathways (typically with five images) and migration barriers of defects are investigated by the climbing-image nudged elastic band (CI-NEB) method [20,21], as implemented within the Vienna Ab-initio Simulation Package (VASP) code [22]. The computational methods employed to confirm the initial and final states haves been previously described in detail elsewhere

* Corresponding author at: Department of Materials Science and Engineering, University of Tennessee, Knoxville, TN 37996, USA.
E-mail address: wjweber@utk.edu (W.J. Weber).

http://dx.doi.org/10.1016/j.scriptamat.2017.06.003
1359-6462/

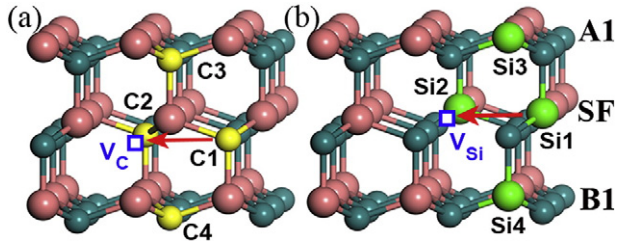

Fig. 1. The positions of the second neighbor C (1–4) (yellow spheres) and Si (1–4) (light green spheres) atoms relative to (a) the C vacancy and (b) the Si vacancy (blue boxes), respectively. The migration pathway for C1 to V_c in (a) is shown by the arrow; likewise, the migration pathway for Si1 to V_{Si} in (b) is shown by the arrow. The pink and dark green spheres represent the Si and C sublattice atoms, respectively.

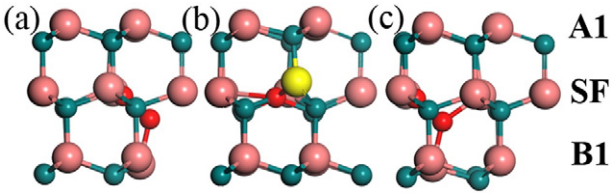

Fig. 2. Migration of C interstitial along the SF layer, (a) initial interstitial $C_{sp\ \langle 110\rangle}$, (b) transition state C-Si $_{\langle 110\rangle}$, (c) final interstitial $C_{sp\ \langle 110\rangle}$. The red sphere is the C interstitial atom; the yellow sphere is the displaced Si atom.

[19]. Different charge states of these point defects have been considered based on our previous work [19].

For both C and Si vacancies, four migration pathways, parallel (path 1 and 2) and perpendicular (path 3 and 4) to the SF layer, are considered, as shown in Fig. 1. The energy barriers along these pathways are given in Table 1. It is interesting to note that the migration barriers for the C vacancy along the SF layer are lower than those in the orthogonal direction. This behavior can be explained by the asymmetrical relaxation near the SF layer [19,23]. Specifically, the small local strain field introduced by SFs causes the Si atoms surrounding the C vacancies to displace outward along the perpendicular direction [19]. This makes the distance between the second C neighbors and C-site vacancy in the parallel direction shorter than that in the perpendicular direction, and thus lowers the migration barrier along the SF layer. Analogous results can also be found in the case of the Si vacancy. In addition, compared with the mobility of vacancies in bulk 3C-SiC, we find that the migration barriers for both vacancies along the SF layer are lower than those in the bulk, indicating that the existence of SFs enhances the mobility of vacancies in the parallel direction. However, the high migration barriers for vacancies in both the SF and bulk suggest that the mobility of vacancies may be not the underlying mechanism of the enhanced defect annihilation. Besides the second neighbor hops, the transformation of the Si vacancy with its nearest-neighbor atoms, such as $V_{Si} \leftrightarrow V_C$-$C_{Si}$ [24–26], is also considered, as shown in Table 1. In the parallel direction, it is found that the barriers for defect transformation are much higher than those for second neighbor diffusion paths; however, contrasting results can be observed in the orthogonal direction, especially for the neutral charge state. In addition, these barriers for transformations near the SF are higher than those in the bulk, suggesting that the existence of SFs inhibits the transformation of V_{Si} into the complex defect V_C-C_{Si}.

For the C interstitials near the SF layer, the initial and final states were determined in our previous study [19]: the $C_{sp\ \langle 110\rangle}$ is the lowest energy configuration within the SF layer, and the $C_{sp\ \langle 100\rangle}$ is the preferred configuration above or below the SF layer. Since no other configurations near the SF layer have been found, we only consider the direct hop mechanism between the most stable sites. By performing a saddle point search for charge states from +1 to −1, we obtain all the possible migration pathways, including the directions parallel and perpendicular to the SF layer. As shown in Fig. 2, the lowest energy pathway for the diffusion of the $C_{sp\ \langle 110\rangle}$ along the SF layer direction is for one of C interstitials in the dumbbell configuration, close to a neighboring Si atom, to form a metastable C-Si split interstitial, as shown in Fig. 2(b). This C-Si split interstitial rotates to allow the C interstitial to jump to the neighboring C site to form a new $C_{sp\ \langle 110\rangle}$, and the displaced Si atom returns to its original position. For the diffusion of the $C_{sp\ \langle 100\rangle}$ along the SF direction, similar results are found, regardless of the charge state. In fact, when considering similar properties for $C_{sp\ \langle 100\rangle}$ and $C_{sp\ \langle 110\rangle}$, as discussed in Ref [19], the comparable migration barriers for both configurations are reasonable. All of these lowest migration barriers are summarized in Table 2.

In the perpendicular direction, the migration behavior follows a similar process as those in the parallel cases, except that the initial and final

Table 1
The migration barriers for vacancies in the bulk and SF region. The values in the parentheses are the migration barriers in the opposite direction. Barriers are in the unit of eV.

		Migration pathway	+2	+1	0	−1	−2
SF	$V_C \leftrightarrow V_C$	1	4.76(4.76)	3.89(3.89)	3.12(3.12)	2.94(2.94)	
		2	4.75(4.75)	3.89(3.89)	3.12(3.12)	2.94(2.94)	
		3	5.25(5.25)	4.30(4.40)	3.53(3.56)	3.37(3.39)	
		4	5.20(5.30)	4.35(4.41)	3.66(3.61)	3.61(3.54)	
	$V_{Si} \leftrightarrow V_{Si}$	1			3.05(3.05)	2.78(2.78)	2.57(2.57)
		2			3.05(3.05)	2.78(2.78)	2.57(2.57)
		3			4.12(4.05)	4.12(4.00)	3.88(3.70)
		4			4.09(4.07)	4.04(4.11)	3.74(3.80)
	$V_{Si} \leftrightarrow V_C$-$C_{Si}$	//			3.72(4.50)	3.93(3.52)	
		⊥			3.54(4.07)	4.10(3.32)	
Bulk	$V_C \leftrightarrow V_C$		5.50[a]	4.42[a]	3.36[a]	3.44[a]	
			5.2[b]	4.1[b]	3.5[b]		
					3.66[c]		
	$V_{Si} \leftrightarrow V_{Si}$			3.93[a]	3.78[a]	3.67[a]	2.74[a]
				3.6[b]	3.4[b]	3.2[b]	2.4[b]
							2.7[c]
	$V_{Si} \leftrightarrow V_C$-$C_{Si}$				2.73(3.87)[a]	3.91(3.40)[a]	
					2.4(3.5)[b]	2.5(2.4)[b]	

[a] This work.
[b] Reference [24].
[c] Reference [27].